

Contents lists available at ScienceDirect

Corrosion Science

journal homepage: www.elsevier.com/locate/corsci



Exploring the effect of amino acid and glucose on the biodegradation of pure Zn



Xiao Liu^a, Yan Cheng^a, Zhenpeng Guan^{c,**}, Yufeng Zheng^{a,b,*}

- ^a Academy for Advanced Interdisciplinary Studies, Peking University, Beijing, 100871, PR China
- b Department of Materials Science and Engineering, College of Engineering, Peking University, Beijing, 100871, PR China
- ^c Orthopedics Department, Peking University Shougang Hospital, No.9 Jinyuanzhuang Rd, Shijingshan District, 100144, Beijing, PR China

ARTICLE INFO

Keywords:

A. Zinc

C. Biodegradation

A. Amino acid

A. Glucose

A. Buffer system

ABSTRACT

To take insights into the participation of amino acid $_{\text{L}}$ -glutamine and glucose in the biodegradation of pure Zn, immersion tests and electrochemical approaches were conducted in designated electrolytes. It revealed that two organic components affected the Zn biodegradation distinctly and played significant parts in the formation of biodegradation products. In media buffered with Tris-HCl, solution pH was effectively adjusted while the involvement of organic components in the Zn biodegradation got noticeably altered. Moreover, with the introduction of two organic components, Tris-HCl buffered SBF may yield better replication of the in vivo biodegradation of zinc.

1. Introduction

During last few years, the research on biodegradable zinc have made some progress and received increasing acceptance as a new generation of promising candidates for biodegradable medical implants. Numerous in vivo experiments have been conducted in various animal models to elucidate the potential of pure Zn [1–3] and its alloys such as Zn-Mg alloys [4], Zn-Li alloys [5] and Zn-Cu alloys [6], as well as metal matrix composites like Zn-HA [7], targeting for the usage in cardiovascular intervention and bone repair. The results revealed benign biodegradability and mechanical strength of Zn-based alloy, as well as suitable degradation rate matching to the tissue healing pace, which almost meet the clinic requirements for ideal biodegradable metallic implants [2].

Despite the prevalence of in vivo experiments to assess the implants, high financial and ethical burdens restricted its scope of practice. In fact, in term of the degradation properties, feasible and cost-effective in vitro approaches such as immersion tests, the hydrogen evolution and electrochemical tests can be utilized before the clinal trials. However, a gap exists between the in vitro and the in vivo corrosion performance of Zn and its alloys [8]. In the human body, the biodegradation behaviour of Zn is synergically affected by environment, microstructure, post-processing and corrosion product [9]. Among them, the sophisticated physiological environment containing inorganic ions, organic molecules, proteins, cells, localized pH values and O₂, imposes remarkable

influence on the biodegradation of implants [10]. Accordingly, to understand and clarify the biodegradation mechanism of Zn, this field of research attracts growing attention and comparative studies are carried out in NaCl solution, simulated body fluid (SBF), phosphate borate solution (PBS), plasma and whole blood [11–13]. Moreover, to better predict the corrosion behaviour of implants in vivo, developing a reliable corrosive medium for in vitro tests is urgently desired. SBF buffered with Tris (hydroxymethyl) aminomethane was suggested as a promising choice to characterize the early stage degradation behaviour of zinc [13]. Exposed to SBF with Tris-HCl buffer system, pure Zn displayed comparable corrosion rate, corrosion product and corrosion morphology to that in vivo and the solution pH was maintained at the physiological range. However, the influence of organic components such as amino acids, vitamins, protein or glucose on the degradation of zinc is out of consideration herein.

It's said that organic components can affect the formation of corrosion product during the biodegradation of magnesium, and the influence of amino acids [14–17] and glucose [18–20] have been considerably investigated. It's reported that amino acids could accelerate the corrosion of pure Mg [14] and promote the mineralization of phosphate [15], and the isoelectric points and molecular structures of amino acids might induce the variations of solution pH [16]. Meanwhile, Willumeit et al. [21] claimed that the glucose was the least important factor to simulate the in vivo tests of biodegradable Mg through artificial neural network analysis. However, Zeng et al.

E-mail addresses: guanzhenpeng@qq.com (Z. Guan), yfzheng@pku.edu.cn (Y. Zheng).

^{*} Corresponding author at: Academy for Advanced Interdisciplinary Studies, Peking University, Beijing, 100871, PR China.

^{**} Corresponding author.

[18–20] elucidated the vital role the glucose played in the degradation process of pure Mg and Mg-Ca alloys. In the saline solution, the glucose affected the corrosion behaviour of Mg content-dependently. In Hanks' solution, the glucose preferred the formation of Ca-P compounds and improved the corrosion resistance of magnesium [18,19]. Moreover, the glucose could transform into the gluconic acid, lowering the solution pH during the immersion and greatly altering the Mg degradation. Actually, the effect that amino acids and glucose exerted on the degradation behaviour of Zn already raised concerns [22]. The introduction of organic components to the in vitro conditions might be the next approach to better understanding the biodegradation processes of Zn. Till now, however, the roles of amino acid and glucose in the biodegradation of zinc are barely understood and nearly no investigation is carried out.

In this study, $_{\rm L}$ -glutamine ($_{\rm L}$ -Gln) and glucose were added into the SBF with or without Tris-HCl buffer system. $_{\rm L}$ -Gln is the most abundant free amino acid in the human body and plays a regulatory role in several physiological functions [23]. It has the concentration about 0.568 mmol/L in the human blood plasma [24]. Glucose, widely accepted as the primary nutrient to maintain and promote the cell function, has a concentration about 1.1 g/L in the human blood plasma [25]. Immersion tests, corrosion product characterization and electrochemical tests were performed on pure Zn in these designated solutions. The aim was to elucidate the individual and synergistic influence of organic components, pH value and buffer system on the biodegradation of Zn.

2. Experimental

2.1. Sample preparation

The pure zinc (with purity of $99.99\,\text{wt.\%}$) rod samples extruded from ingots at $250\,^\circ\text{C}$ and at a reduction ratio of 16, were cut into $1.0\,\text{mm}$ thick discs with $1.0\,\text{cm}$ diameter. The specimens were mechanically wet ground with silicon carbide abrasive paper successively from 800 to 2000 grits before they were ultrasonically cleaned for $5\,\text{min}$ in acetone and another $5\,\text{min}$ in ethanol. Then, the specimens were dried in air under sterile conditions.

2.2. Immersion tests

Simulated body fluid (SBF) with or without Tris – HCl buffer system were selected as the base media for immersion tests. L-glutamine (Gibco, Invitrogen) and glucose were added with the same concentration in human blood plasma. The concentration of inorganic and organic components in six electrolytes and the human blood plasma were listed in Table 1. The non-buffered SBF was prepared with the following composition: 8.035 g/L NaCl, 0.355 g/L NaHCO₃, 0.225 g/L KCl, 0.231 g/L K₂HPO₄·3H₂O, 0.311 g/L MgCl₂·6H₂O, 0.292 g/L CaCl₂ and

 $0.072\,g/L~Na_2SO_4$. The initial pH was adjusted to 7.42 with the help of NaOH and HCl. The buffered SBFs were prepared with extra 6.118 g/L Tris and the solution pH was adjusted to 7.42 with HCl. The immersion tests were then carried out at 37 °C for 1, 3, 7, 14, 28 and 56 days without electrolyte renewal. The ratio of solution volume to surface area was about $20\,\text{mL/cm}^2$. During the test, the medium pH was monitored continuously and recorded at different time intervals. At least 3 parallel samples were prepared for each time point to verify the reproducibility.

After immersion tests, samples at certain time points were taken out, cleaned with distilled water and dried in the air. The solution containing $200\,\mathrm{g/L}$ CrO_3 was used to remove the corrosion product from surface. Specimens were then washed by water and ethanol, and dried at the room temperature. Sample weights were determined prior to and after the removal of corrosion products. The corrosion rate (C) was derived from weight loss according to ASTM-G31-12a:

$$C = (K \times W) / (A \times T \times D) \tag{1}$$

where C is in units of mm/yr, the coefficient $K = 8.76 \times 10^4$, W is the mass loss, D is the material density (g), A is the exposed surface area (mm²), and T is the time of immersion (h).

2.3. Corrosion product characterization

To characterize the surface morphology and elemental distribution of corrosion product on sample surface after immersion, the environmental electron microscopy (ESEM, Thermal Fisher Quattro S, USA) coupled with energy-disperse spectrometer (EDS) was employed, operating at an acceleration voltage of 15.00 kV. Constituents of corrosion products on the surface were examined by means of X-ray diffractometer (XRD) and performed on a Powder X-ray diffractometer (XRD, X-Pert3 Powder, Netherlands). Diffraction patterns were generated continuously from 10° to 90° in 20 at a speed of 4°/min. Fourier transform infrared spectroscopy (FTIR, Nicolet Is50, USA) was used to analyse the chemical constituents and the spectra were collected in 400 – 4000 cm⁻¹. X-ray photoelectron spectroscopy (XPS, Kratos Analytical Inc., UK) with a monochromated Al Ka X-ray source operating at 150 W was utilized to determine the surface chemistry. The survey spectra were acquired at a pass energy of 160 eV and the region spectra were recorded at 40 eV pass energy. The data analysis was performed by using the CasaXPS software version 2.3.16. All the spectra were shown after energy calibration and the reference peak was the C1s peak at 284.8 eV.

2.4. Electrochemical experiments

Electrochemical measurements were conducted in designated electrolytes at room temperature with an electrochemical workstation (Autolab, Metrohm, Switzerland) and a three-electrode cell set-up was

 $\begin{tabular}{ll} \textbf{Table 1} \\ \textbf{The chemical composition of human blood plasma and electrolytes (mmol/L)}. \\ \end{tabular}$

	Human Plasma	SBF	SBF + Gln	SBF + Glucose	SBF (Tris-HCl)	SBF (Tris-HCl) + Gln	SBF (Tris-HCl) + Glucose
Na ⁺	142	142	142	142	142	142	142
K ⁺	5.0	5.0	5.0	5.0	5.0	5.0	5.0
Mg^{2+}	1.5	1.5	1.5	1.5	1.5	1.5	1.5
Ca ²⁺	2.5	2.6	2.6	2.6	2.6	2.6	2.6
Cl-	103	149	149	149	> 149	> 149	149
HCO ₃ -	27.0	4.2	4.2	4.2	4.2	4.2	4.2
HPO ₄ ²⁻	1.0	1.0	1.0	1.0	1.0	1.0	1.0
SO ₄ ²⁻	0.5	0.5	0.5	0.5	0.5	0.5	0.5
Tris	_	_	_	_	50.5	50.5	50.5
_L -Gln	0.56	_	0.56		_	0.56	_
Glucose	5	_	_	5.5	_	_	5.5

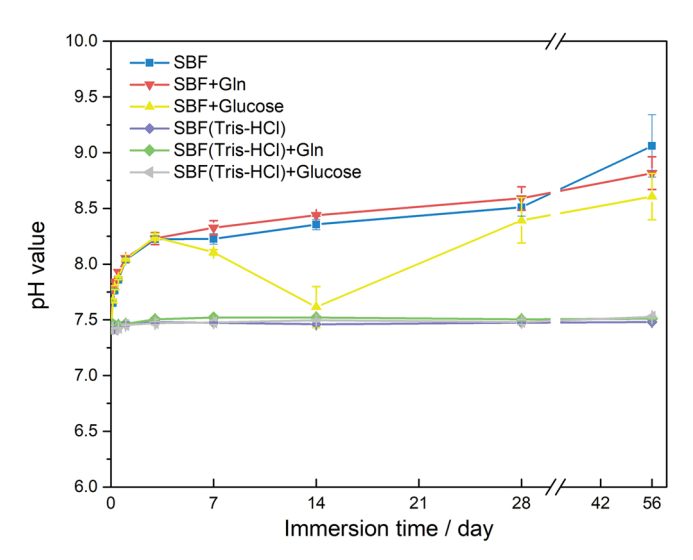


Fig. 1. Evolution of pH values as a function of immersion time.

utilized. The saturated calomel electrode (SCE) and a platinum electrode were used as the reference electrode and the counter electrode, respectively. The open circuit potential (OCP) was recorded for the first 3600 s. The Electrochemical Impedance Spectroscopy measurement (EIS) was performed in a frequency range from 10^5 Hz to 10^{-2} Hz by applying 2 mV perturbation to OCP values, in consideration of the reactive nature of zinc. The potentiodynamic polarization tests (PDP) were carried out with a scan rate of 1 mV/s. Each test was repeated at least three times to check the reproducibility.

3. Results

3.1. Immersion tests

3.1.1. Change of solution pH

Fig. 1 displays the variations of pH values in buffer-free and Tris-HCl buffered SBFs with $_{\rm L}\text{-}Gln$ or glucose added during 56 days of immersion. In buffer-free SBF, solution pH increased steeply in the initial 3 days, and then manifested a slow growth trend with the elapse of immersion. With the introduction of $_{\rm L}\text{-}Gln$, the media pH exhibited higher value and slightly fluctuated during 28 days of immersion. After 56 days, solution pH was considerably lowered by $_{\rm L}\text{-}Gln$. In contrast, the impact of glucose on the pH value was insignificant initially. 3 days later, the media pH decreased immensely and reached the lowest value after 14 days. Then, the solution pH increased again and remained constant up with time, and exhibited the lowest value among three buffer-free SBFs. In the meantime, as indicted in Fig. 1, pH values of three Tris-HCl buffered SBFs was effectually controlled by the buffer system and maintained at the range of 7.45–7.50. $_{\rm L}\text{-}Gln$ and glucose mildly raised the solution pH.

3.1.2. Weight loss and corrosion rate

In Fig. 2, the weight loss and corrosion rate of pure Zn after 1, 3, 7, 14, 28 and 56 days of immersion were shown. The mean values and the standard deviations of the parallel samples are displayed. During 14 days of exposure in buffer-free SBF, pure Zn experienced increasing weight loss and decreasing degradation rate with the elapse of time. Afterwards, the degradation of pure Zn accelerated sharply and the average corrosion rate for 56-day immersion was about 0.049 $\rm mm\cdot yr^{-1}$, highest among three SBFs. With the addition of $_{\rm L}$ -Gln or glucose, the degradation of pure Zn got encouraged in 14 days but the corrosion rate decreased with time. Afterthat, the degradation rate of pure Zn increased slowly and exhibited lower value than that in non-buffered SBF. The average corrosion rate for 56-days immersion with $_{\rm L}$ -Gln or glucose

was about $0.023 \,\mathrm{mm\cdot yr^{-1}}$ and $0.014 \,\mathrm{mm\cdot yr^{-1}}$, respectively.

With the introduction of Tris-HCl buffer system, the degradation rate of pure Zn in three SBFs was remarkably raised, as shown in Fig. 2(d). The weight loss of samples in three electrolytes increased continually and the corrosion rate diminished with time. $_{\rm L}$ -Gln promoted the dissolution of Zn and increased the corrosion rate, despite the impact became insignificant after 56 days. In contrast, the glucose retarded the Zn degradation throughout the immersion. During 56 days of immersion, the average corrosion rate of pure Zn in Tris-HCl buffered SBF was approximately 0.033 mm·yr $^{-1}$. In the presence of $_{\rm L}$ -Gln or glucose, the average corrosion rates were about 0.034 mm·yr $^{-1}$ and 0.027 mm·yr $^{-1}$, respectively.

3.2. Surface morphology after immersion

In Fig. 3, the surface morphology of samples immersed in three buffer-free SBFs is revealed. After 1 day of exposure in SBF, the sample surface was almost intact. As time prolonged, the surface was populated with a myriad of white corrosion product. The precipitations accumulated and agglomerated with time. After 28 days, a layer of corrosion product was covered on the surface and can be identified in Fig. 3A. Then, the precipitates continued nucleating and growing on the layer. After 56 days, white globular precipitations were evenly distributed over the product layer. Identification of the selected area and representative corrosion product after 56 days of immersion was attempted by EDX analysis, as shown in Table 2. It turned out that the surface layer and corrosion product formed during the immersion test were mainly composed of Zn, O, C, Ca, P and Mg. With L-Gln added in SBF, the corrosion product was formed immediately and dispersed on the sample surface just after 1 day, despite the surface morphology kept nearly unchanged in the following 14 days. As the immersion time extended, white precipitations piled up and agglomerated after 28 days, and the surface morphology barely changed during another 28 days of exposure. The corrosion product layer was almost invisible in Fig. 3B and EDX analysis also revealed that the elemental compositions of the surface layer formed after 1 day and 56 days were quite similar. In the meantime, the glucose slightly affected the formation of corrosion product on pure Zn surface during 7 days of immersion in SBF. Then, after 14 days, a dense layer of corrosion product was formed, as shown in Fig. 3C. Clusters of white precipitations were covered on it, which continually deposited and grew with time.

Fig. 4 depicts the SEM surface morphology images of pure Zn immersed in three buffered SBFs. After 7 days of exposure in Tris-HCl buffered SBF, nearly no corrosion product was generated on sample surface and the appearance of surface kept unvaried. Afterwards, a myriad of corrosion products gradually nucleated and accumulated. With the introduction of $_{\rm L}$ -Gln or glucose, the white precipitates was formed in advance and can be recognized on the surface after 7 days. During the following immersion, the glucose slightly enhanced the deposition of corrosion product and the impact of $_{\rm L}$ -Gln became neglectable. Furthermore, after 56-day exposure in three buffered SBFs, a thin film underneath the white precipitate was covered on the surface. Additionally, the corrosion product formed in three electrolytes was all composed of Zn, Ca, P, C and O (Table 3).

3.3. Corrosion product characterization after immersion

Fig. 5 describes the XRD spectra of pure Zn after 56 days of immersion. It turned out that ZnO and CaCO $_3$ were the main crystallized product formed in six electrolytes. The peak-shift emerged in several profiles and it might be ascribed to the uneven settlement of sample. To give a deeper insight into the composition of degradation product, FTIR spectra of samples after 56 days of immersion were collected, as demonstrated in Fig. 6. The band at $560\,\mathrm{cm}^{-1}$ likely originated from metal oxides and implied the possible existence of ZnO [26]. Characteristic absorption band of PO $_4$ 3- at $580\,\mathrm{cm}^{-1}$ was assigned to the ν_4

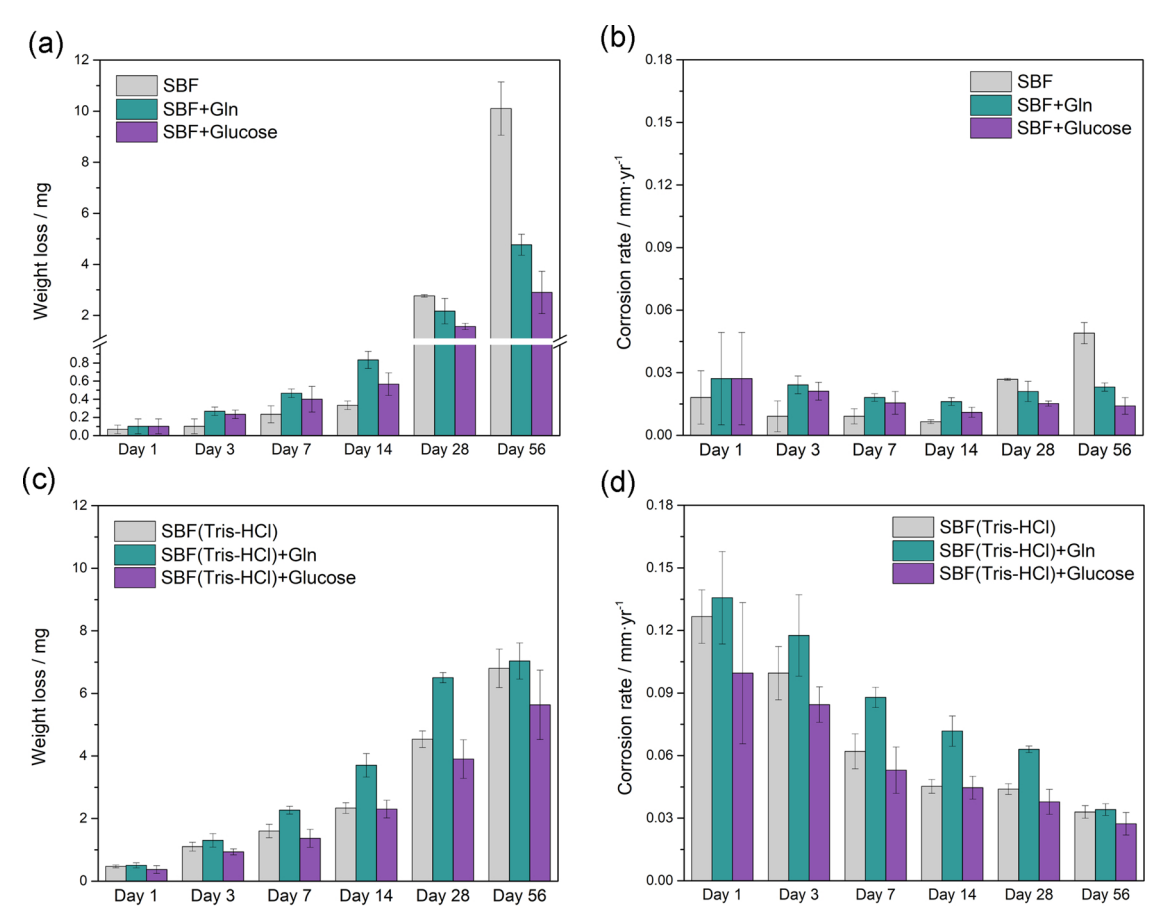


Fig. 2. Weight loss and derived degradation rate of pure Zn as a function of time.

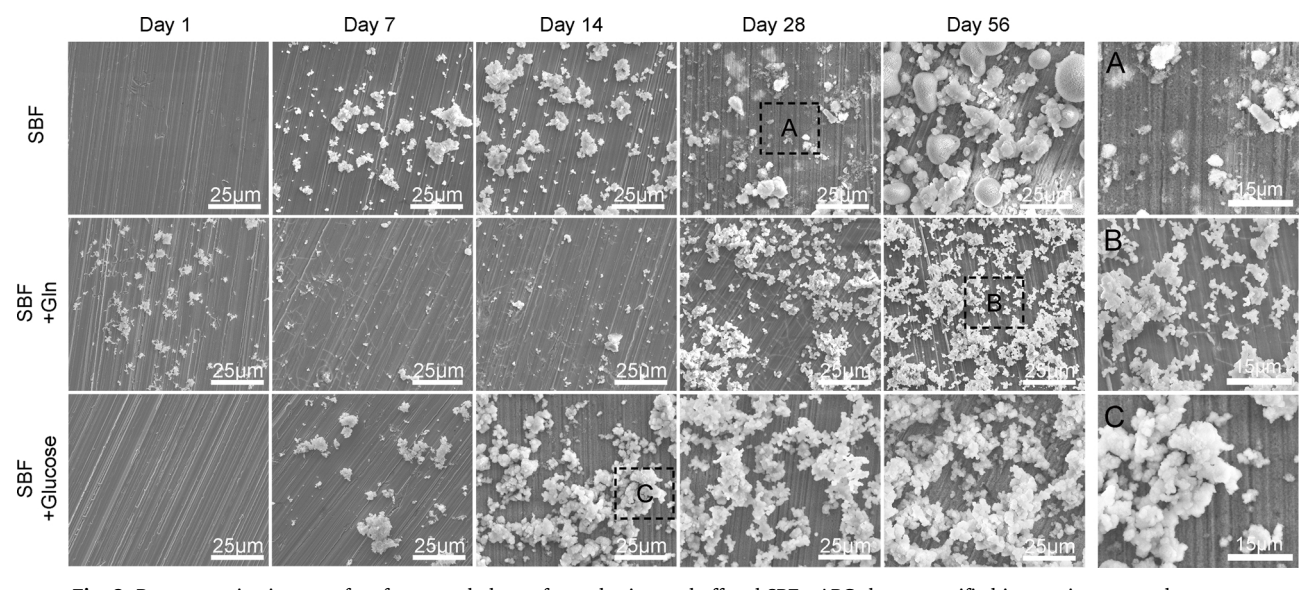


Fig. 3. Representative images of surface morphology of samples in non-buffered SBFs. ABC show magnified images in rectangular areas.

vibrational mode [27] and the intensive absorption band from 920 to $1100 \, \mathrm{cm}^{-1}$ was attributed to the v_3 vibrational mode [11]. A series of bands from 1380 to $1590 \, \mathrm{cm}^{-1}$ can be ascribed to the $\mathrm{CO_3}^{2-}$ antisymmetric stretching modes of v_3 [28]. The band located at $1640 \, \mathrm{cm}^{-1}$ was related to the bending vibration mode of water molecules, and the broad one at $3100-3500 \, \mathrm{cm}^{-1}$ was assigned to the O–H stretching vibration [29]. In summary, the corrosion product was mainly composed of carbonates, phosphates and zincite. With the existence of Tris-HCl buffer system, the formation of carbonates in SBF was restrained.

Meanwhile, $_{\rm L}\text{-}Gln$ remarkably raised the intensity of characteristic peaks of PO $_{\rm 4}^{\rm 3-}$ in corrosion product formed in two kinds of SBFs. The glucose also favoured the formation of phosphates, albeit with less impact compared to $_{\rm L}\text{-}Gln.$

To further investigate the chemical nature of corrosion product, XPS was carried out on samples ($\sim\!10$ nm) after immersion for 56 days [30]. As shown in Fig. 7, element Zn, O, C, Ca, P and Mg appeared in the survey spectra. After deconvolution, the curve fits of Zn $2p_{3/2}$, P 2p and Ca 2p are displayed in Figs. 8 and 9. In term of Zn $2p_{3/2}$, the single peak

Table 2Results of EDS analysis of sample morphology in three SBFs (at. %).

	Zn	О	С	Ca	P	Mg	Cl
SBF							
Day 1- surface	65.7	9.1	23.7	0.6	0.9	_	_
Day 7- surface	53.4	18.1	21.0	2.6	0.9	0.9	-
Day 7- white precipitations	11.5	43.5	14.7	15.3	12.5	2.5	-
Day 56- product layer	27.0	42.7	13.8	8.6	6.2	1.6	-
Day 56-white precipitations	6.0	49.8	6.7	23.6	12.3	1.5	
$SBF + _{L}-Gln$							
Day 1- surface	40.6	29.1	17.2	5.2	5.9	1.9	-
Day 1- white precipitations	4.8	57.4	11.1	13.6	10.7	2.5	-
Day 56- product layer	39.8	31.1	17.4	4.6	5.4	1.7	-
Day 56- white precipitations	2.5	51.1	5.8	23.9	14.7	2.1	-
SBF + Glucose							
Day 1- surface	66.0	7.0	23.5	0.6	3.0	-	-
Day 7- surface	57.8	12.4	24.3	1.5	3.2	0.9	-
Day 7- white precipitations	17.1	42.1	17.6	11.1	9.8	2.3	-
Day 56- product layer	30.1	43.7	12.8	6.2	6.6	0.6	-
Day 56- white precipitations	11.0	52.5	13.4	11.9	10.6	0.6	-

located at $1021.6-1021.9\,\mathrm{eV}$ was attributed to ZnO [31,32]. The peak at $1021.6\,\mathrm{eV}$ suggested the existence of $\mathrm{Zn}_5(\mathrm{CO}_3)_2(\mathrm{OH})_6$ [33] and the one at $1021.8\,\mathrm{eV}$ can be characterized as $\mathrm{Zn}(\mathrm{OH})_2$ [34]. The Ca 2p spectra shown in Fig. 8 involved two peaks and the one at $347.3-347.6\,\mathrm{eV}$ can be assigned to the calcium phosphate [35]. The P 2p spectra consisting of one single peak was located at $133.3-133.5\,\mathrm{eV}$, corresponding to $\mathrm{PO_4}^{3-}$ [36] and further confirming the precipitation of the phosphate compounds [35]. Therefore, after 56-day exposure in six electrolytes, the corrosion products on the very surface were primary ZnO and calcium phosphate. In several electrolytes, hydrozincite and zinc hydroxide might also be existed. Besides, the intensity of P 2p and Ca 2p was extremely low in SBF and the addition of two organic components raised their intensity. In the presence Tris-HCl, the intensity of P 2p was raised and two organic components reduced the intensity of Ca characteristic peak.

3.4. Electrochemical measurements

3.4.1. Open circuit potential

The OCPs of samples during 3600 s of immersion in six electrolytes were recorded. The representative curves were selected and shown in Fig. 10. In three buffer-free SBFs, a gradual increase in the corrosion potential followed by the downward trend emerged during the initial

Table 3Results of EDS analysis of sample morphology in three Tris-HCl buffered SBFs (at. %).

	Zn	O	С	Ca	P	Mg	C1
SBF (Tris-HCl)							
Day 7- surface	62.8	10.3	22.7	0.6	3.6	_	-
Day 14- surface	56.2	18.3	20.3	1.4	3.8	-	-
Day 14- white precipitations	37.7	34.9	17.5	3.2	6.0	0.8	-
Day 56- product layer	44.7	35.1	15.3	1.5	3.4	-	-
Day 56- white precipitations	16.6	50.7	13.8	4.5	8.3	0.7	5.5
SBF (Tris- HCl) + $_L$ - Gln							
Day 1- surface	69.9	4.2	23.1	_	2.7	_	-
Day 7- surface	58.1	15.8	21.1	1.2	3.8	-	-
Day 7- white precipitations	30.5	37.6	19.3	4.2	7.5	0.9	-
Day 56- product layer	41.9	36.8	15.1	2.1	4.1	-	-
Day 56- white precipitations	18.4	53.6	13.8	4.7	8.8	0.7	-
SBF(Tris-HCl) + Glucose							
Day 1- surface	68.5	3.6	25.1	_	2.8	_	-
Day 7- surface	59.2	14.9	21.4	1.1	3.4	_	-
Day 7- white precipitations	32.5	34.6	20.9	3.9	7.3	0.8	-
Day 56- product layer	39.6	38.5	14.7	2.4	4.7	-	-
Day 56- white precipitations	16.5	55.3	14.8	4.3	8.4	0.7	-

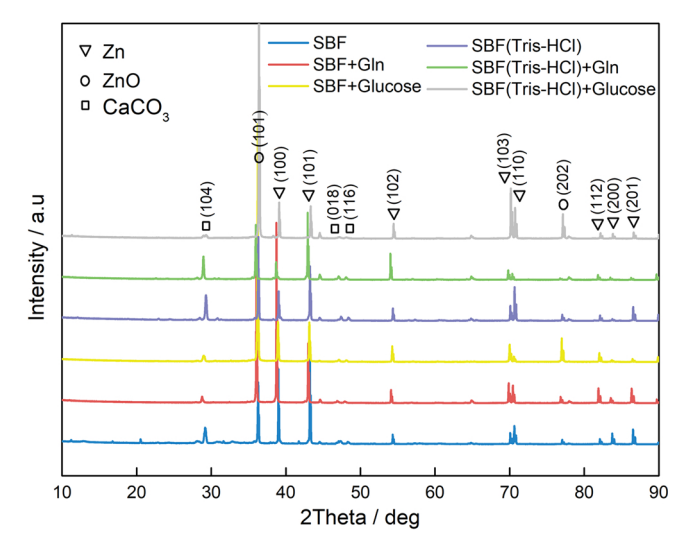


Fig. 5. XRD spectra of corrosion product after 56 days of immersion.

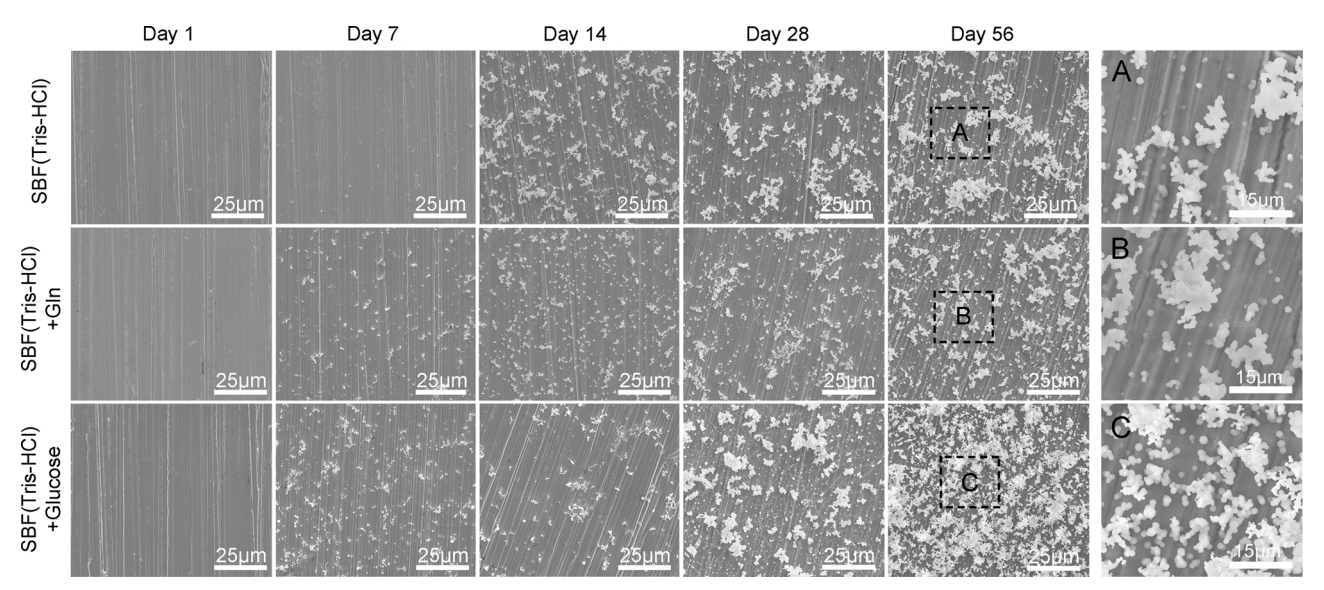


Fig. 4. Representative images of surface morphology of samples in Tris-HCl buffered SBFs. ABC show magnified images in rectangular areas.

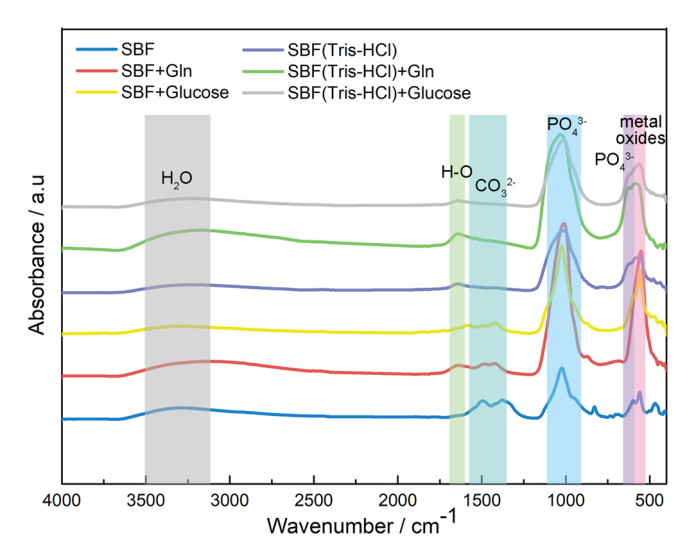


Fig. 6. FTIR spectra of corrosion product after 56 days of immersion.

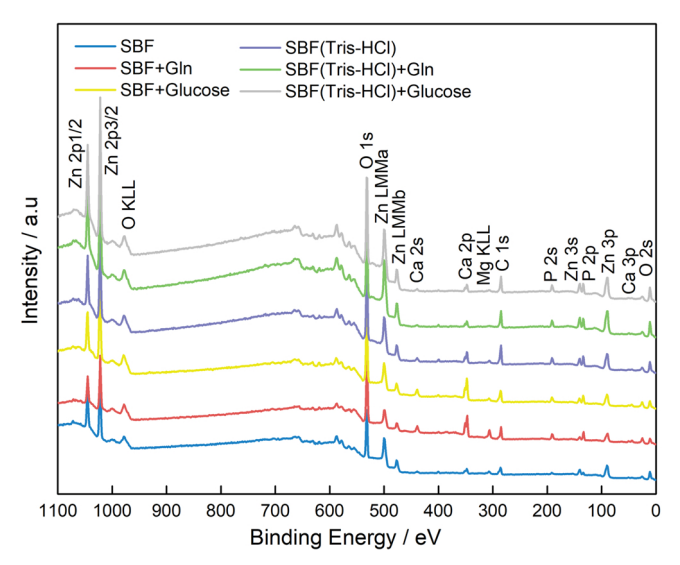


Fig. 7. XPS survey of corrosion product after 56 days of immersion.

stage of exposure. It might be correlated with the dissolution of the initially grown film on pure Zn [37]. In the presence of L-Gln, the overall OCP shifted negatively, signifying the loss of surface stability. However, no large fluctuations in the potentials were observed in SBF with or without I-Gln, denoting the general corrosion processes involved in two electrolytes [38]. By comparison, the glucose altered the thermodynamic stability of samples in SBF. The corrosion potential considerably fluctuated during 1800s of exposure and drifted continuously to more noble direction due to the piecemeal deposition of corrosion product [39]. In three Tris-HCl buffered SBFs, the variations in the potential during open-circuit exposure manifested quite similar tendency. The potential was inclined to the positive value in the beginning and then remarkably dropped. Afterthat, the OCP remained constant up and approached a steady state step by step, despite of intensive fluctuations caused by the precipitation and dissolution of the corrosion product [38].

3.4.2. Potentiodynamic polarization

Fig. 11 presents the PDP curves of samples exposed to designated electrolytes. With respect to samples in three SBFs, $_{\rm L}$ -Gln and glucose mildly increased the corrosion potential, suggesting the reduced sensitivity of Zn to corrosion attack after the cathodic polarization in the presence of organic components [40]. The cathodic parts of three

polarization curves were alike and indicated the existence of several cathodic reactions involved. And L-Gln and glucose mildly accelerated the cathodic reactions. Regarding three anodic branches in Fig. 11(a), pure Zn experienced a rapid acceleration of anodic dissolution and then a protective-like passivation with elevated potential. L-Gln lowered the anodic dissolution rate. It's deduced that the corrosion product formed during the polarization might possess higher protectivity with L-Gln present. Regarding samples exposed to Tris-HCl buffered solutions, as depicted in Fig. 11(b), the corrosion potential positively drifted in the presence of two organic components, as a result of potentially formed protective corrosion product. In addition, the cathodic part of the polarization curves appeared untypical Tafel relations with the introduction of 1-Gln or glucose. In this study, the media was stationary and non-deaerated, and the dominant cathodic reaction of zinc in nearneutral media was the oxygen reduction [41]. Therefore, the reduction of oxygen might be affected by two organic components. Besides, with two kinds of organic compounds added, the passive-like region and the breakdown point emerged in the anodic polarization curve and the anodic dissolution current was suppressed. The corrosion rates calculated based on the anodic part of polarization curves are listed in Table 4. Without buffer system, L-Gln and glucose both promoted the degradation of pure Zn in SBF. In Tris-HCl buffered solution, L-Gln decreased the corrosion rate of pure Zn and the glucose still facilitated the Zn dissolution.

3.4.3. Electrochemical impedance spectroscopy

Electrochemical impedance spectroscopy (EIS) was performed on samples exposed to designated electrolytes to estimate the electrode corrosion resistance and investigate the processes occurring at the electrode/electrolyte interface. The impedance response of pure Zn after 1 h of immersion are illustrated in Fig. 12. The Nyquist plots showed two time constants in three buffer-free SBFs, including one high frequency capacitance loop and one low frequency capacitance loop. Two capacitance loops corresponded to the characteristics of the electric double layer and formed passive layer, respectively. The dimensions of the high frequency loop dwindled with the existence of organic components and displayed the minimal value with L-Gln addition, denoting the reduced corrosion resistance of pure Zn. Meanwhile, with regard to the impedance response of samples in Tris-HCl buffered SBFs, two well-defined semicircles can be distinguished in Fig. 12(b) and corresponded to two time constants at high and low frequencies, respectively. Noticeably, in comparison to that in Fig. 12(a), the diameter of Nyquist plots in three buffered SBFs got pronouncedly decreased and the influence of L-Gln and glucose became insignificant.

In consequence, the impedance response of pure Zn in six electrolytes manifested similar patterns with diverse dimensions, signifying the comparable electrochemical processes with varied degree of reaction resistance in the electrolyte/electrode interface. Thus, a two-time constant electrical equivalent circuit (EEC) was employed to interpret the impedance response in Fig. 12 and a good fit was obtained. To better model the electrode capacitive behaviour, a constant phase element (CPE) was utilized to compensate the non-ideal capacitive behaviour induced by factors such as surface roughness and heterogeneities, slow adsorption, electrode porosity, or the nonuniform potential and current distribution [42]. The impedance of a CPE can be given by the following equation:

$$Z_{CPE} = Q^{-1}(j\omega)^{-n} \tag{2}$$

where Z_{CPE} is the CPE impedance $(\Omega\,cm^2)$, Q is a constant $(\Omega\,cm^2\cdot s^n)$, j is the imaginary number and ω is the angular frequency $(\omega=2\pi f,f)$ is the frequency). n is a dimensionless constant in the range of $-1 \le n \le 1$. Note that n=1 corresponds to the ideal capacitance, a resistor yields n=0, an inductor yields n=-1 and n=0.5 yields the response of mass transport processes.

The fitting results are listed in Table 5. R_s is identical to the electrolyte resistance. R_{ct} and CPE₁ refer to the charge transfer resistance

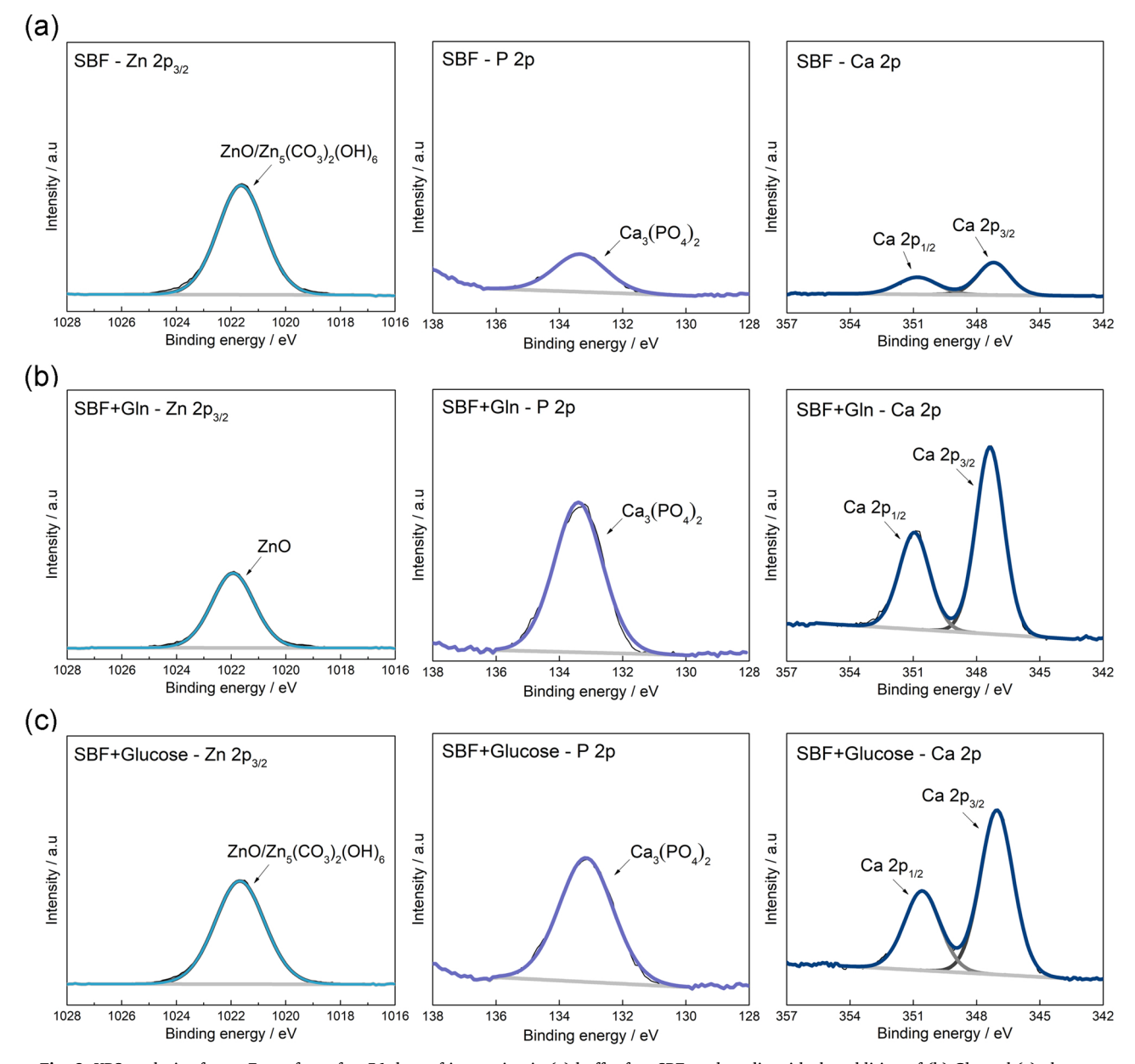


Fig. 8. XPS analysis of pure Zn surface after 56 days of immersion in (a) buffer-free SBF, and media with the addition of (b) Gln and (c) glucose.

and the electric double layer capacity at the interface of substrate and electrolyte, respectively. $R_{\rm f}$ and CPE₂ represent the resistance and capacitance of the corrosion product film, respectively. In addition, the diameter of the capacitive loop was reported to directly proportional to the film resistance for mass transfer and charge transfer resistance, and the sum of $R_{\rm f}$ and $R_{\rm ct}$ was considered as the polarization resistance $R_{\rm p}$ [43]. Accordingly, $R_{\rm p}$ in buffer-free SBF decreased as follows: glucose > SBF > L-Gln. The corrosion resistance of pure Zn during the early immersion stage in SBF was lowered by Tris-HCl, and $R_{\rm p}$ reduced as follows: glucose > L-Gln > SBF (Tris-HCl).

4. Discussion

4.1. Corrosion mechanism of pure Zn in SBF with or without Tris-HCl buffer system

The corrosion mechanisms of pure Zn in six electrolytes were proposed, as shown in Fig. 13. In SBF, the dissolution of zinc took place immediately after exposure to water, accompanied by the reduction of

oxygen as the primary cathodic reaction. The released Zn^{2+} and OH^{-} in aqueous solution lead to the formation of $\mathrm{Zn}(\mathrm{OH})_2$, and then more thermodynamically stable ZnO was formed [1]. In addition, $\mathrm{Zn}(\mathrm{OH})_2$ can re-dissolve into Zn^{2+} due to the chloride attack [44].

$$Zn \rightarrow Zn^{2+} + 2e^{-} \tag{3}$$

$$O_2 + H_2O + 4e^- \rightarrow 4OH^-$$
 (4)

$$Zn^{2+} + 2OH^{-} \rightarrow Zn(OH)_{2}$$
 (5)

$$Zn(OH)_2 \rightarrow ZnO + H_2O \tag{6}$$

$$Zn(OH)_2 + 2Cl^- \rightarrow Zn^{2+} + 2OH^- + 2Cl^-$$
 (7)

$$5Zn(OH)_2 + 2HCO_3^- + 2H^+ \rightarrow Zn_5(CO_3)_2(OH)_6 + 4H_2O$$
 (8)

$$3Ca^{2+} + 2PO_4^{3-} \rightarrow Ca_3(PO_4)_2$$
 (9)

The by-product OH⁻ of cathodic reaction lead to the constantly increased pH values. The electrolyte lacked the ability to control the solution alkalization and thus pH values far exceeded 9.0 at last. After 28 days, the continuous accumulation of precipitations contributed to

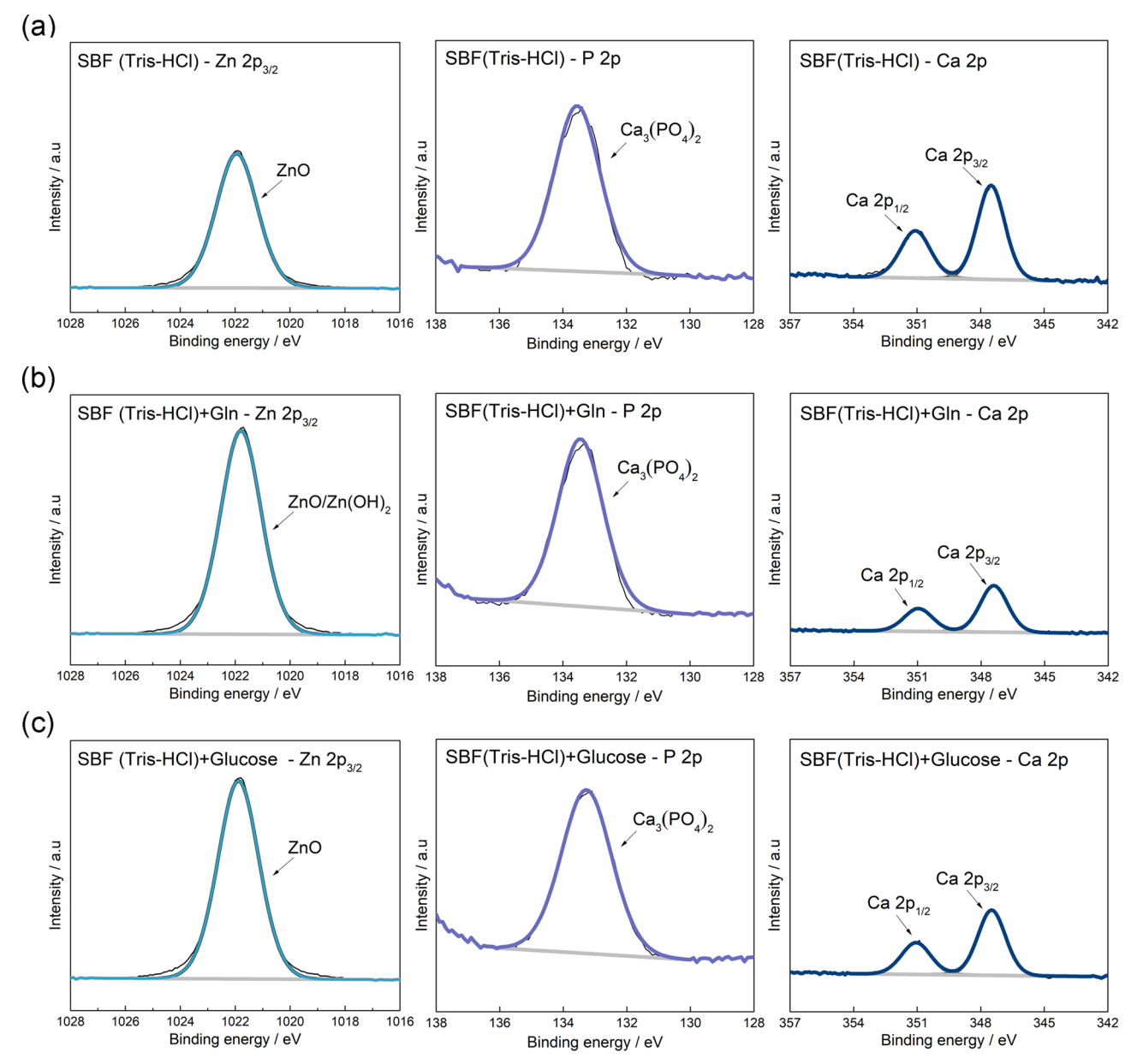


Fig. 9. XPS analysis of pure Zn surface after 56 days of immersion in (a) Tris-HCl buffered SBF, and media with the addition of (b) Gln and (c) glucose.

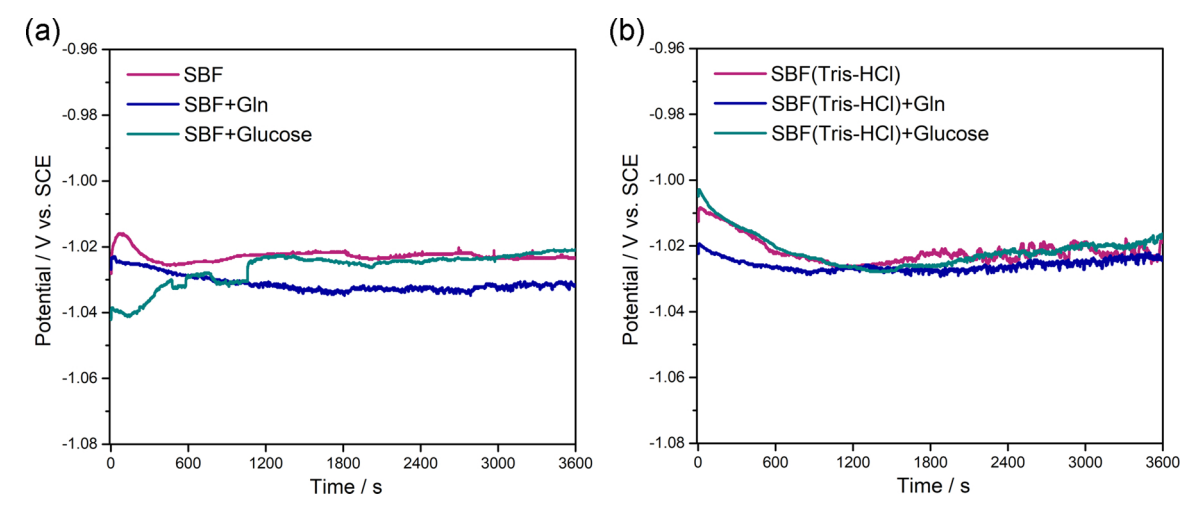


Fig. 10. Open circuit potential vs. time of pure Zn in (a) buffer-free and (b) Tris-HCl buffered SBFs.

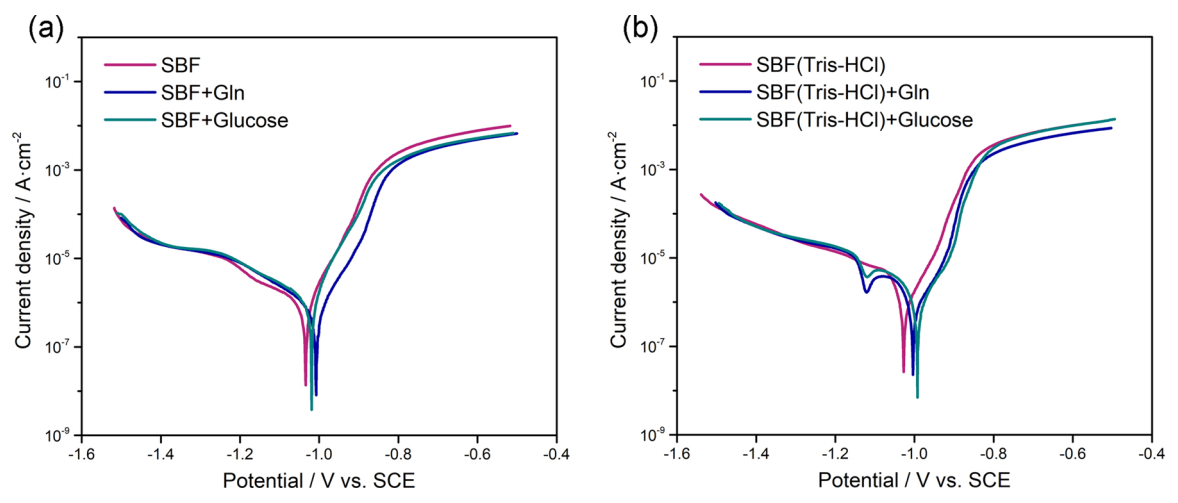


Fig. 11. Potentiodynamic polarization curves of pure Zn in (a) buffer-free and (b) Tris-HCl buffered SBFs.

Table 4 Electrochemical parameters of PDP curves in six kinds of electrolytes.

	$E_{\rm corr}$ / V vs. SCE	$i_{\rm corr}$ / ($\mu {\rm A~cm}^{-2}$)	P _i / (mm/year)
SBF	-1.033	3.241	0.048
SBF + Gln	-1.005	4.135	0.062
SBF + Glucose	-1.009	5.675	0.084
SBF(Tris-HCl)	-1.024	4.119	0.061
SBF(Tris-HCl) + Gln	-1.004	2.951	0.044
SBF(Tris-HCl) + Glucose	-0.999	4.815	0.072

the formation of corrosion product layer on the surface. The change in the surface morphology was likely to affect the mass transport and the diffusion of ions and oxygen. The corrosion mode varied and the degradation of pure Zn accelerated progressively. The carbonates were precipitated on the surface [45], and the coexistence of Ca²⁺ and PO₄³⁻ gave rise to the precipitation of calcium phosphate [46].

The Tris-HCl buffer system was claimed to be able to maintain a pH range from 7.0–9.0 [20]. The hydrolysis of the amino-group of Tris gave rise to the pH value [47], while bonded H $^+$ in Tris-HCl depleted hydroxide anion and retarded the augment of solution pH. In this study, the solution pH was effectively controlled in 56 days and sustained in the range acceptable in the human body. Meanwhile, it's reported that Tris-HCl could prevent the precipitation of HCO_3^- , HPO_4^{2-} , H_2PO_4^- and SO_4^{2-} salts [47], and light complexations formed between Tris and Zn^{2+} [48], as well as Tris and Ca^{2+} [49]. Hence, the generation of

corrosion product was retarded and the dissolution of Zn was promoted by Tris-HCl. Pure Zn exhibited faster degradation in SBF in the presence of Tris-HCl. The corrosion rate and the polarization resistance $R_{\rm p}$ obtained from the electrochemical tests also unveiled the increscent defeated nature of pure Zn in buffered SBF. However, with the elapse of immersion, the corrosion products were deposited on the sample surface unceasingly. The corrosion resistance of pure Zn was gradually improved and eventually, the average corrosion rate for 56-day immersion in SBF was lowered by Tris-HCl.

4.2. The influence of organic components on the corrosion behaviour of pure Zn

4.2.1. The corrosion mechanism of pure Zn in the presence of $_L$ -Gln

In buffer-free SBF, the addition of $_{\rm L}$ -Gln lowered the open circuit potential and polarization resistance $R_{\rm p}$ of samples at the initial immersion stage. Pure Zn became more vulnerable to the corrosion attack in the presence of $_{\rm L}$ -Gln and the Zn dissolution was encouraged. The corrosion rate derived from the potentiodynamic polarization and the immersion test both exhibited higher values with $_{\rm L}$ -Gln present. The continuous release of ${\rm Zn}^{2+}$ in solution induced the corrosion product formation, which nucleated and deposited on the surface immediately after 1 day. For the following 14 days, the degradation of pure Zn was still accelerated but the deposition of precipitations was remarkably inhibited by $_{\rm L}$ -Gln. It's said that the complex-formation occurred

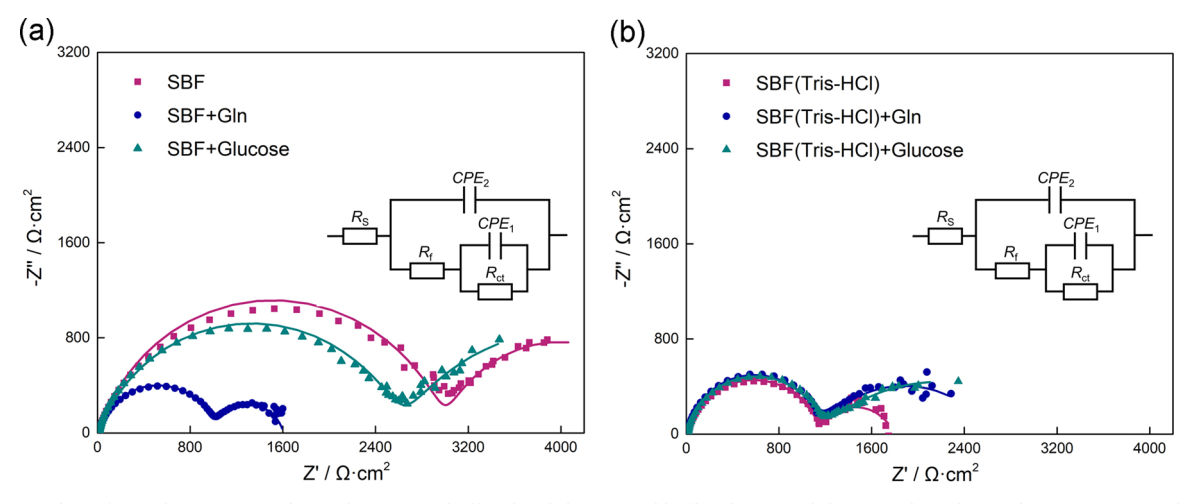


Fig. 12. Nyquist plots of impedance spectra obtained in (a) non-buffered and (b) Tris-HCl buffered SBFs and the equivalent electrical circuit (EEC) used to fit the EIS data. The scatter implied data points and the line fitted data.

Table 5The fitted results of electrochemical impedance spectra in six electrolytes.

	$R_{\rm s}~(\Omega{\rm cm}^2)$	$R_{\rm ct}~(\Omega{\rm cm}^2)$	$R_{\rm f} (\Omega {\rm cm}^2)$	CPE_1-Q $(\Omega^{-1}\cdot s^n cm^{-2})$	CPE ₁ -n	CPE_2 -Q (Ω^{-1} ·s ⁿ cm ⁻²)	CPE ₂ -n
SBF	12.3	3002.6	1985.1	8.10E-06	0.81	4.56E-03	0.83
SBF + Gln	11.3	1012.9	580.4	5.25E-06	0.85	1.23E-03	0.85
SBF + Glucose	10.0	2625.6	2848.2	1.11E-05	0.78	4.51E-03	0.68
SBF(Tris-HCl)	9.5	1140.6	640.6	4.47E-06	0.86	2.46E-03	0.77
SBF(Tris-HCl) + Gln	10.8	1135.1	1495.8	5.29E-06	0.91	1.60E-03	0.63
SBF(Tris-HCl) + Glucose	11.3	1134.7	2084.6	6.05E-06	0.89	2.23E-03	0.51

between Zn²⁺ and L-Gln [24], which might facilitate the dissolution of precipitations in this work and prevent their formation from taking place [50]. At the same time, L-Gln was unstable in the media with prolonged immersion, and it might deaminate into ammonia with time [51]. Ozturk et al. [52] also reported the glutamine decomposition rate constants as a function of pH in the range of 6.7–7.8 in different cell culture media, the higher media pH, the less remained L-Gln. Hence, with extending time and growing pH values, the amount of L-Gln in solution might decrease and their inhibition effect on the corrosion product formation might be relieved. Therefore, after 28 days, the sample surface was populated with white precipitations although the product film was un-recognizable after 56 days.

In Tris-HCl buffered SBF, the introduction of L-Gln slightly affected the pH-control ability of buffer system and the solution pH was maintained at the desired range. The biodegradation of Zn was promoted by L-Gln and corrosion product was deposited in advance. However, after 7 days, the influence of L-Gln on the corrosion morphology became insignificant. As time prolonged, the Zn degradation slowed down and it might be related to the accumulation of corrosion products. Ultimately, L-Gln barely affected the average corrosion rate of pure Zn for 56 days of immersion in buffered SBF.

It can be speculated that the participation of $_{\rm L}$ -Gln in the biodegradation process of pure Zn was altered by Tris-HCl. Comparing the polarization curves of pure Zn in two SBFs with $_{\rm L}$ -Gln existed, the cathodic branch illustrated disparate characteristics. The cathodic reactions involved such as the oxygen reduction might be influenced by Tris-HCl, as well. Theoretically, the role of $_{\rm L}$ -Gln in the degradation process can be affected by pH value, ionic strength, temperature, chemical composition of media, etc [52]. The media pH was not only

closely relevant to the decomposition of glutamine, but also of importance to the bonding between amino acids and metal surface [53]. In addition, in the research of biodegradable Mg, it's reported that after the solution pH became stable, $_{\rm L}\text{-}{\rm Gln}$ took part in the degradation process of pure Mg by the adsorption or other ways and its concentration decreased with time [15]. Hence, the pH variations caused by Tris-HCl in SBF might alter the Zn biodegradation in various ways. More importantly, Tris-HCl itself can stimulate the decomposition of $_{\rm L}$ -Gln at the alkaline solution [54]. It came to a conclusion that the degradation of pure Zn might be synergically influenced by $_{\rm L}$ -Gln, pH value and Tris-HCl, and therefore behaved distinctly in two kinds of SBFs.

4.2.2. The corrosion mechanism of pure Zn in the presence of glucose

During the initial stage of immersion in buffer-free SBF, the glucose barely affected the degradation behaviour of pure Zn. The open circuit potential and the impedance response was slightly varied. For 1 day of immersion, the glucose made no difference to the surface morphology and solution pH, but encouraged the degradation of Zn noticeably. After 3 days, the solution pH dropped greatly and reached the lowest value after 14 days. The transformation of glucose into gluconic acid might be relevant to the acidification of media [18]. The reduced pH accelerated the dissolution of pure Zn and enabled the formation of massive corrosion product. Hence, a corrosion product layer was formed on the surface subsequently. Nonetheless, with prolonged immersion, the acidity got overwhelmed by the generation of cathodic reduction by-product OH⁻, and the pH values increased again. The corrosion resistance of pure Zn got enhanced due to the protective precipitates and finally, the average corrosion rate for 56-day

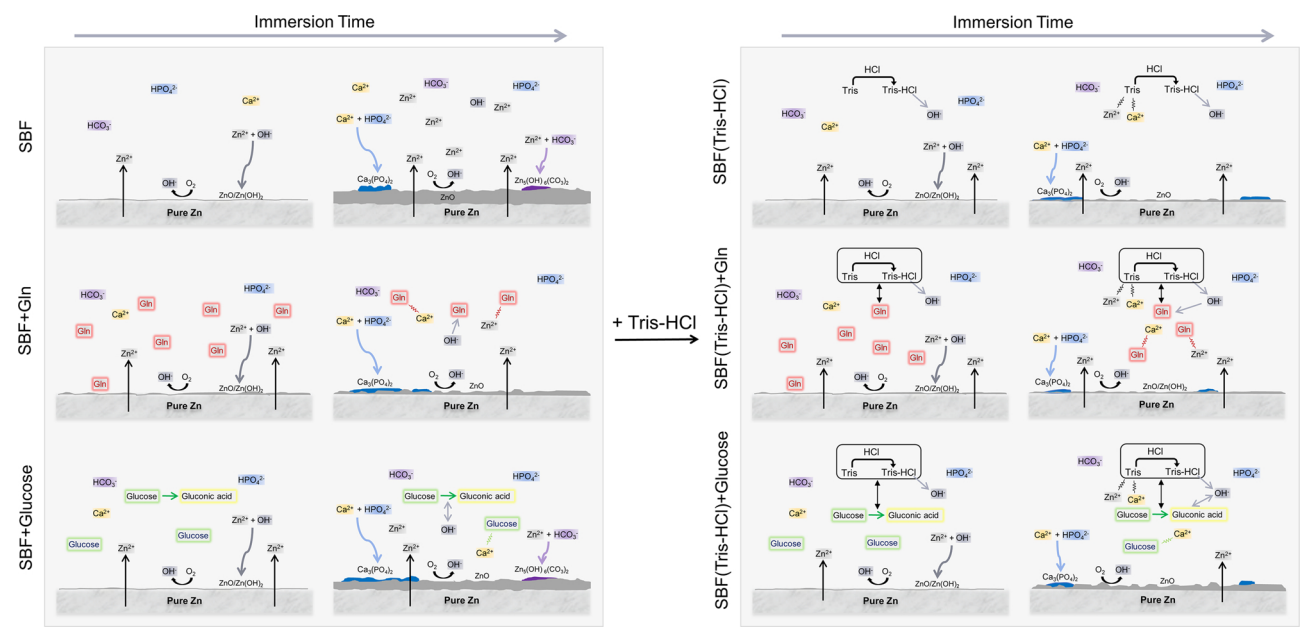


Fig. 13. Schematic illustration of the degradation of pure Zn in buffer-free SBFs and Tris-HCl buffered SBFs.

immersion was lowered by glucose.

In SBF buffered with Tris-HCl, the media pH was sustained at the values about 7.47 for the whole immersion. The buffer ability of Tris-HCl was insignificantly affected by glucose and the acidification induced by the transformation of glucose was eliminated. The participation of glucose in the biodegradation of pure Zn was changed by Tris-HCl. The corrosion product formation was favoured by glucose, the corrosion resistance got improved and pure Zn displayed the lowest corrosion rate among three buffered SBFs.

4.3. Evaluation of Tris-HCl buffered SBF system to mimic in vivo degradation

To screen the biodegradable Zn and its alloys from an in vitro corrosion perspective, developing the feasible in vitro models is a pressing need to replicate the sophisticated in vivo microenvironments of human body in artificial. It's reported that an effective and applicable simulation of the in vivo conditions required similar corrosion rate, corrosion product and corrosion morphology [10]. Till now, literatures on the in vivo degradation behaviour of pure Zn were already available. The in vivo studies by Bowen et al. [2,3] highlighted the outstanding biocompatibility and biodegradability of pure Zn wire in the rat aorta and claimed ZnO and zinc carbonates as the primary degradation product after 4.5 months of implantation. In the meantime, by implanting pure Zn stents in the abdominal aorta of rabbit, the present authors' lab [1] revealed a uniform corrosion pattern of pure Zn and an average degradation rate about 0.03 mm·yr⁻¹ for 1 month of implantation. In addition, a layer of corrosion product consisting of ZnO and Zn₃(PO₄)₂·4H₂O was identified on the surface. What's more, to systematically appraise the potential of Zn for orthopaedic implant applications, a rat femur condyle model was employed and the biodegradation behaviour of pure Zn in bone environments was investigated [7]. After 4 weeks, the implantation was surrounded by newly formed bone and pure Zn displayed a uniform corrosion mode without severe localized corrosion. More importantly, the degradation products exhibited two-layer structure after 8 weeks. The inner layer was comprised of oxidized constituents and carbonates and the outer layer contained extra Ca-P salts.

4.3.1. The influence of immersion time

It's reported that pure Zn degraded at an average rate about 0.04 mm·yr⁻¹ for 14 days of immersion in Tris-HCl buffered SBF and the corrosion product had comparable chemical composition to that in vivo [13]. It came to a provisional conclusion that Tris-HCl buffered SBF can characterize the initial corrosion behaviour of Zn properly. To further explore and assess the reliability of such combination, the immersion time was extended to 56 days here. In non-buffered SBF, the corrosion mode of pure Zn changed after 28 days and the Zn degradation accelerated impressively. In contrast, pure Zn went through a decreasing degradation rate with prolonged time in Tris-HCl buffered SBF and corroded uniformly. The average corrosion rate for 56 days of immersion was about 0.034 mm yr⁻¹. The corrosion product primarily consisting of ZnO and Ca₃(PO₄)₂ was evenly distributed over the sample surface. EDX analysis and FTIR spectra revealed the existence of phosphates after 56 days of immersion, however, the formation of Zn₃(PO₄)₂ cannot be confirmed. Overall speaking, the biodegradation of pure Zn during 56-day exposure in Tris-HCl buffered SBF can still match the pace in vivo.

4.3.2. The influence of organic components

In order to elucidate the participation of organic components in the biodegradation processes of pure Zn and take a step towards a closer simulation of in vivo environment, organic components were introduced into the Tris-HCl buffered SBF. It turned out that the pH-control ability of Tris-HCl was mildly affected by L-Gln and glucose, and the solution pH can still be managed at desired range. The Zn

degradation in buffered SBF was immensely accelerated by $_{\rm L}$ -Gln in 28 days, but the average degradation rate for 56-day immersion was slightly affected by $_{\rm L}$ -Gln and about 0.034 mm·yr $^{-1}$. In contrast, the degradation rate of pure Zn in buffered SBF was moderately lowered by the glucose for 56 days of exposure and manifested an average value about 0.027 mm·yr $^{-1}$.

During the immersion in buffered SBF, the corrosion morphology and the corrosion pattern of pure Zn was slightly influenced by L-Gln and glucose. By comparison, these two organic components made a difference to the chemical composition of corrosion products. The formation of phosphates was noticeably encouraged by L-Gln in two kinds of SBF and the similar effect was elucidated during the biodegradation of Mg in Hanks' balanced salt solution (HBSS) [15]. The glucose also marginally favoured the precipitation of phosphates. More importantly, the content of calcium element in the corrosion product on the very surface was reduced. It uncovered that the precipitation of Ca-P compounds in Tris-HCl buffered SBF was restrained by L-Gln and glucose. It's said that the treatment with amino acids can prevent the calcification effectively [55]. Qin et al. [56] investigated the complex formed between Ca²⁺ and common amino acids systematically. The Gln-Ca²⁺ complex was found in possession of the highest stability. What's more, L-Gln could interact with the active growth site of the hydroxyapatite and thus inhibit the growth of hydroxyapatite crystal [55]. The glucose was also considered as the chelating agent for Ca2+ in aqueous solutions and it might inhibit the precipitation of calcium compounds [57]. In the meantime, the in vivo experiments revealed that the outer layer of corrosion product rich in Ca-P salts was formed on pure Zn only after 6 months of implantation in the abdominal aorta of rabbit [1]. Besides, the calcification was viewed as the most common cause of clinical failures of cardiac valve bioprostheses [55]. Therefore, due to their inhibition effect on the Ca-P salts precipitation in buffered SBF, L-Gln and glucose might be able to give a closer simulation to the corrosion product formation during the artery remodelling.

For biodegradable Mg, the researches exploring the influence of 1-Gln and glucose on the in vitro degradation mechanism of Mg and its alloys were already in progress. It unveiled that the absorbed amino acids on the surface preferred the mineralization of hydroxyapatite during Mg degradation [58], and the L-Gln under cell culture conditions favoured the formation of phosphates and Ca-P salts, despite the interaction between L-Gln and inorganic ions PO₄³⁻/Ca²⁺/Mg²⁺ remained unclear [15]. Similarly, the glucose could coordinate with Ca²⁺ in Hanks' solution and thereby stimulate the precipitation of Ca-P compounds on the Mg surface [18]. In conclusion, L-Gln and glucose were both beneficial for the mineralization of Ca-P compounds during the degradation of Mg. As a matter of fact, it should be noted that none of these studies were carried out in the presence of buffer system, irrespective of the individual and collaborative influence of buffer itself and media pH on the Ca-P precipitation. What's more, it's claimed that the amount of calcium phosphate in the corrosion product layer depended on the material of implant [44]. The in vivo experiments of Mg revealed that the calcium phosphate can completely replace the strut section of magnesium-based stents. On the contrary, the calcium phosphate on zinc implants was only a few microns thick [1], owing to the inhibition effect of Zn on the formation of soluble calcium phosphate and the growth of phosphate layer [59]. It came to an instructive conclusion herein that to benefit from the research experience in biodegradable Mg properly, the experimental details and the distinct characteristics of materials should be take into consideration.

To summarize, Tris-HCl buffered SBF can still be recommended for the future evaluation of degradation behaviour of Zn and its alloys, and the introduction of organic components can be adopted for in vitro biocorrosion testing to obtain more reliable results, especially for the materials designed for usage within blood vessel.

4.4. New aspects and outlooks

In the physiological environment of an adult human, due to the fluid exchange by the excretion of urine [14], the concentration of the biodegradation product in the body fluid, as well as inorganic and organic components, can be regulated by the homeostatic processes. However, in in vitro experiments, the accumulation of released ions and the depletion of free ions in the electrolytes might vary the media pH, the corrosion product formation and the degradation rate. Moreover, the increase in the solution pH and concentration of free $\rm Zn^{2+}$ can influence the solubility equilibrium of inorganic ions such as $\rm Ca^{2+}$, $\rm HCO_3^-$ and $\rm HPO_4^{2-}$, which were tightly connected with the protectivity of the corrosion product layer and even the corrosion mode.

In this study, the immersion tests were conducted without electrolyte renewal. The concerns about the increscent pH values can be erased by the utilization of Tris-HCl buffer system [9], but the differences made by the accumulation of corrosion product and the consumption of free inorganic ions were out of scope. Zinc phosphates were the main corrosion product formed during the in vivo degradation of pure Zn [1]. But it cannot be identified on the very surface of samples after the whole immersion. Besides, the depletion of available L-Gln was likely to change the corrosion behaviour of pure Zn during the later stage of immersion in two SBFs. Actually, Ascencio et al. [60] had investigated the effect of daily electrolyte renewal on the corrosion mechanism and kinetics of WE43 Mg alloy in the modified SBF. It turned out that the concentration of relevant electrolyte components was better emulated through the renewal of electrolyte. Accordingly, the solubility of the corrosion product was affected, the layer protectivity was changed and the occurrence of localized corrosion were delayed. Consequently, the corrosion mechanism of WE43 Mg alloy was altered. Therefore, aseptically removing and replenishing the fluid with the fresh one to sustain the constant concentration of electrolyte components might be the next step to gain a deeper insight into the corrosion mechanism of Zn and its alloys in vivo.

5. Conclusions

The degradation behaviour of pure Zn in two kinds of SBFs with $_{\rm L^-}$ Gln or glucose addition was systematically investigated, and the following conclusions can be drawn:

- (1) In non-buffered SBF, L-Gln facilitated the degradation of pure Zn and noticeably retarded the corrosion product formation. By comparison, the glucose accelerated the Zn degradation and promoted the deposition of corrosion product.
- (2) In buffered SBFs, _L-Gln and glucose made an insignificant difference to the pH-control ability of Tris-HCl and pH values of three SBFs were sustained at desired range. However, the involvement of _L-Gln and glucose in the corrosion mechanism of pure Zn was altered by Tris-HCl. For 56-day immersion, _L-Gln and glucose slightly affected the average degradation rate of pure Zn, but inhibited the formation of Ca-P compounds.
- (3) With the introduction of $_{\rm L}$ -Gln and glucose, Tris-HCl buffered SBF can better replicate and predict the in vivo Zn degradation, and might be a better option for the in vitro Zn characterization for cardiovascular application.

CRediT authorship contribution statement

Xiao Liu: Conceptualization, Investigation, Data curation, Writing original draft. Yan Cheng: Writing - review & editing, Supervision. Zhenpeng Guan: Resources, Supervision. Yufeng Zheng: Conceptualization, Writing - review & editing, Supervision, Project administration, Funding acquisition.

Declaration of Competing Interest

The authors declare that they have no known competing financial interests or personal relationships that could have appeared to influence the work reported in this paper.

Acknowledgements

This work was supported by the National Key R&D Program of China (2018YFE0104200), and the National Natural Science Foundation of China (Grant No.51931001).

Appendix A. Supplementary data

Supplementary material related to this article can be found, in the online version, at doi:https://doi.org/10.1016/j.corsci.2020.108661.

References

- [1] H. Yang, C. Wang, C. Liu, H. Chen, Y. Wu, J. Han, Z. Jia, W. Lin, D. Zhang, W. Li, W. Yuan, H. Guo, H. Li, G. Yang, D. Kong, D. Zhu, K. Takashima, L. Ruan, J. Nie, X. Li, Y. Zheng, Evolution of the degradation mechanism of pure zinc stent in the one-year study of rabbit abdominal aorta model, Biomaterials 145 (2017) 92–105, https://doi.org/10.1016/j.biomaterials.2017.08.022.
- [2] P.K. Bowen, J. Drelich, J. Goldman, Zinc exhibits ideal physiological corrosion behavior for bioabsorbable stents, Adv. Mater. 25 (2013) 2577–2582, https://doi. org/10.1002/adma.201300226.
- [3] P.K. Bowen, R.J. Guillory 2nd, E.R. Shearier, J.M. Seitz, J. Drelich, M. Bocks, F. Zhao, J. Goldman, Metallic zinc exhibits optimal biocompatibility for bioabsorbable endovascular stents, Mater. Sci. Eng. C Mater. Biol. Appl. 56 (2015) 467–472, https://doi.org/10.1016/j.msec.2015.07.022.
- [4] H. Jin, S. Zhao, R. Guillory, P.K. Bowen, Z. Yin, A. Griebel, J. Schaffer, E.J. Earley, J. Goldman, J.W. Drelich, Novel high-strength, low-alloys Zn-Mg (< 0.1wt% Mg) and their arterial biodegradation, Mater. Sci. Eng. C Mater. Biol. Appl 84 (2018) 67–79, https://doi.org/10.1016/j.msec.2017.11.021.</p>
- [5] S. Zhao, J.M. Seitz, R. Eifler, H.J. Maier, R.J. Guillory 2nd, E.J. Earley, A. Drelich, J. Goldman, J.W. Drelich, Zn-Li alloy after extrusion and drawing: structural, mechanical characterization, and biodegradation in abdominal aorta of rat, Mater. Sci. Eng. C Mater. Biol. Appl. 76 (2017) 301–312, https://doi.org/10.1016/j.msec. 2017.02.167.
- [6] C. Zhou, H.-F. Li, Y.-X. Yin, Z.-Z. Shi, T. Li, X.-Y. Feng, J.-W. Zhang, C.-X. Song, X.-S. Cui, K.-L. Xu, Y.-W. Zhao, W.-B. Hou, S.-T. Lu, G. Liu, M.-Q. Li, J.-y. Ma, E. Toft, A.A. Volinsky, M. Wan, X.-j. Yao, C.-b. Wang, K. Yao, S.-k. Xu, H. Lu, S.-F. Chang, J.-B. Ge, L.-N. Wang, H.-J. Zhang, Long-term in vivo study of biodegradable Zn-Cu stent: a 2-year implantation evaluation in porcine coronary artery, Acta Biomater. (2019), https://doi.org/10.1016/j.actbio.2019.08.012.
- [7] H. Yang, X. Qu, W. Lin, C. Wang, D. Zhu, K. Dai, Y. Zheng, In vitro and in vivo studies on zinc-hydroxyapatite composites as novel biodegradable metal matrix composite for orthopedic applications, Acta Biomater. 71 (2018) 200–214, https:// doi.org/10.1016/j.actbio.2018.03.007.
- [8] G. Katarivas Levy, J. Goldman, E. Aghion, The prospects of zinc as a structural material for biodegradable implants—a review paper, Metals 7 (2017) 402, https://doi.org/10.3390/met7100402.
- [9] N.T. Kirkland, J. Waterman, N. Birbilis, G. Dias, T.B. Woodfield, R.M. Hartshorn, M.P. Staiger, Buffer-regulated biocorrosion of pure magnesium, J. Mater. Sci. Mater. Med. 23 (2012) 283–291, https://doi.org/10.1007/s10856-011-4517-y.
- [10] S. Johnston, M. Dargusch, A. Atrens, Building towards a standardised approach to biocorrosion studies: a review of factors influencing Mg corrosion in vitro pertinent to in vivo corrosion, Sci. China Mater. 61 (2017) 475–500, https://doi.org/10. 1007/s40843-017-9173-7.
- [11] K. Torne, M. Larsson, A. Norlin, J. Weissenrieder, Degradation of zinc in saline solutions, plasma, and whole blood, J. Biomed. Mater. Res. B Appl. Biomater. 104 (2016) 1141–1151, https://doi.org/10.1002/jbm.b.33458.
- [12] Y. Meng, L. Liu, D. Zhang, C. Dong, Y. Yan, A.A. Volinsky, L.-N. Wang, Initial formation of corrosion products on pure zinc in saline solution, Bioact. Mater. (2018), https://doi.org/10.1016/j.bioactmat.2018.08.003.
- [13] X. Liu, H. Yang, P. Xiong, W. Li, H.-H. Huang, Y. Zheng, Comparative studies of Tris-HCl, HEPES and NaHCO3/CO2 buffer systems on the biodegradation behaviour of pure Zn in NaCl and SBF solutions, Corros. Sci. 157 (2019) 205–219, https://doi.org/10.1016/j.corsci.2019.05.018.
- [14] A. Yamamoto, S. Hiromoto, Effect of inorganic salts, amino acids and proteins on the degradation of pure magnesium in vitro, Mater. Sci. Eng. C 29 (2009) 1559–1568, https://doi.org/10.1016/j.msec.2008.12.015.
- [15] R.Q. Hou, N. Scharnagl, F. Feyerabend, R. Willumeit-Romer, Exploring the effects of organic molecules on the degradation of magnesium under cell culture conditions, Corros. Sci. 132 (2018) 35–45, https://doi.org/10.1016/j.corsci.2017.12.023.
- [16] Y. Wang, B.-H. Ding, S.-Y. Gao, X.-B. Chen, R.-C. Zeng, L.-Y. Cui, S.-J. Li, S.-Q. Li, Y.-H. Zou, E.-H. Han, S.-K. Guan, Q.-Y. Liu, In vitro corrosion of pure Mg in phosphate buffer solution—Influences of isoelectric point and molecular structure of amino acids, Mater. Sci. Eng. C (2019), https://doi.org/10.1016/j.msec.2019.110042.

- [17] D. Mei, S.V. Lamaka, C. Feiler, M.L. Zheludkevich, The effect of small-molecule biorelevant organic components at low concentration on the corrosion of commercially pure Mg and Mg-0.8Ca alloy: an overall perspective, Corros. Sci. 153 (2019) 258–271, https://doi.org/10.1016/j.corsci.2019.03.039.
- [18] R.C. Zeng, X.T. Li, S.Q. Li, F. Zhang, E.H. Han, In vitro degradation of pure Mg in response to glucose, Sci. Rep. 5 (2015) 13026, https://doi.org/10.1038/srep13026.
- [19] Y. Wang, L.Y. Cui, R.C. Zeng, S.Q. Li, Y.H. Zou, E.H. Han, In vitro degradation of pure magnesium-the effects of glucose and/or amino acid, Materials (Basel) 10 (2017), https://doi.org/10.3390/ma10070725.
- [20] L.-Y. Li, B. Liu, R.-C. Zeng, S.-Q. Li, F. Zhang, Y.-H. Zou, H.G. Jiang, X.-B. Chen, S.-K. Guan, Q.-Y. Liu, In vitro corrosion of magnesium alloy AZ31 a synergetic influence of glucose and Tris, Front. Mater. Sci. 12 (2018) 184–197, https://doi.org/10.1007/s11706-018-0424-1.
- [21] R. Willumeit, F. Feyerabend, N. Huber, Magnesium degradation as determined by artificial neural networks, Acta Biomater. 9 (2013) 8722–8729, https://doi.org/10. 1016/j.actbio.2013.02.042.
- [22] X. Liu, H.T. Yang, Y. Liu, P. Xiong, H. Guo, H.H. Huang, Y.F. Zheng, Comparative studies on degradation behavior of pure zinc in various simulated body fluids, Jom 71 (2019) 1414–1425, https://doi.org/10.1007/s11837-019-03357-3.
- [23] P. Newsholme, J. Procopio, M.M. Lima, T.C. Pithon-Curi, R. Curi, Glutamine and glutamate-their central role in cell metabolism and function, Cell Biochem. Funct. 21 (2003) 1–9, https://doi.org/10.1002/cbf.1003.
- [24] The computed distribution of copper(II) and zinc(II) ions among seventeen amino acids present in human blood plasma, Biochem. J. 121 (1971) 549–555, https://doi. org/10.0000/PMID5119792.
- [25] M.B. Kannan, H. Khakbaz, A. Yamamoto, Understanding the influence of HEPES buffer concentration on the biodegradation of pure magnesium: an electrochemical study, Mater. Chem. Phys. 197 (2017) 47–56, https://doi.org/10.1016/j. matchemphys.2017.05.024.
- [26] Q. Qu, L. Li, W. Bai, C. Yan, C.-n. Cao, Effects of NaCl and NH4Cl on the initial atmospheric corrosion of zinc, Corros. Sci. 47 (2005) 2832–2840, https://doi.org/ 10.1016/j.corsci.2004.11.010.
- [27] M. Ascencio, M. Pekguleryuz, S. Omanovic, An investigation of the corrosion mechanisms of WE43 Mg alloy in a modified simulated body fluid solution: the influence of immersion time, Corros. Sci. 87 (2014) 489–503, https://doi.org/10.1016/j.corsci.2014.07.015.
- [28] A. Ślósarczyk, Z. Paszkiewicz, C. Paluszkiewicz, FTIR and XRD evaluation of carbonated hydroxyapatite powders synthesized by wet methods, J. Mol. Struct. 744–747 (2005) 657–661, https://doi.org/10.1016/j.molstruc.2004.11.078.
- [29] Y. Zhang, Y. Yan, X. Xu, Y. Lu, L. Chen, D. Li, Y. Dai, Y. Kang, K. Yu, Investigation on the microstructure, mechanical properties, in vitro degradation behavior and biocompatibility of newly developed Zn-0.8%Li-(Mg, Ag) alloys for guided bone regeneration, Mater. Sci. Eng. C 99 (2019) 1021–1034, https://doi.org/10.1016/j. msec.2019.01.120.
- [30] Y. Qiao, W. Zhang, P. Tian, F. Meng, H. Zhu, X. Jiang, X. Liu, P.K. Chu, Stimulation of bone growth following zinc incorporation into biomaterials, Biomaterials 35 (2014) 6882–6897, https://doi.org/10.1016/j.biomaterials.2014.04.101.
- [31] G. Katarivas Levy, A. Kafri, Y. Ventura, A. Leon, R. Vago, J. Goldman, E. Aghion, Surface stabilization treatment enhances initial cell viability and adhesion for biodegradable zinc alloys, Mater. Lett. (2019), https://doi.org/10.1016/j.matlet. 2019.04.006.
- [32] L.S. Dake, D.R. Baer, J.M. Zachara, Auger parameter measurements of zinc-compounds relevant to zinc transport in the environment, Surf. Interface Anal. 14 (1989) 71–75, https://doi.org/10.1002/sia.740140115.
- [33] J. Rodriguez, L. Chenoy, A. Roobroeck, S. Godet, M.G. Olivier, Effect of the electrolyte pH on the corrosion mechanisms of Zn-Mg coated steel, Corros. Sci. 108 (2016) 47–59, https://doi.org/10.1016/j.corsci.2016.02.041.
- [34] G. Ballerini, K. Ogle, M.G. Barthés-Labrousse, The acid-base properties of the surface of native zinc oxide layers: an XPS study of adsorption of 1,2-diaminoethane, Appl. Surf. Sci. 253 (2007) 6860–6867, https://doi.org/10.1016/j.apsusc.2007.01.
- [35] T. Hanawa, S. Hiromoto, K. Asami, Characterization of the surface oxide film of a Co-Cr-Mo alloy after being located in quasi-biological environments using XPS, Appl. Surf. Sci. 183 (2001) 68–75, https://doi.org/10.1016/S0169-4332(01) 00551-7.
- [36] S. Champagne, E. Mostaed, F. Safizadeh, E. Ghali, M. Vedani, H. Hermawan, In vitro degradation of absorbable zinc alloys in artificial urine, Materials (Basel) 12 (2019), https://doi.org/10.3390/ma12020295.
- [37] R.C. Zeng, Y. Hu, S.K. Guan, H.Z. Cui, E.H. Han, Corrosion of magnesium alloy AZ31: the influence of bicarbonate, sulphate, hydrogen phosphate and dihydrogen phosphate ions in saline solution, Corros. Sci. 86 (2014) 171–182, https://doi.org/ 10.1016/j.corsci.2014.05.006.
- [38] W. Ma, Y. Liu, W. Wang, Y. Zhang, Effects of electrolyte component in simulated

- body fluid on the corrosion behavior and mechanical integrity of magnesium, Corros. Sci. 98 (2015) 201–210, https://doi.org/10.1016/j.corsci.2015.05.012.
- [39] F. El-Taib Heakal, A.M. Fekry, M. Abd El-Barr Jibril, Electrochemical behaviour of the Mg alloy AZ91D in borate solutions, Corros. Sci. 53 (2011) 1174–1185, https:// doi.org/10.1016/j.corsci.2010.11.040.
- [40] Y. Xin, K. Huo, H. Tao, G. Tang, P.K. Chu, Influence of aggressive ions on the degradation behavior of biomedical magnesium alloy in physiological environment, Acta Biomater. 4 (2008) 2008–2015, https://doi.org/10.1016/j.actbio.2008.05.
- [41] S. Thomas, N. Birbilis, M.S. Venkatraman, I.S. Cole, Corrosion of zinc as a function of pH, Corrosion-Us 68 (2012) 160–166, https://doi.org/10.5006/1.3676630.
- [42] J.-B. Jorcin, M.E. Orazem, N. Pébère, B. Tribollet, CPE analysis by local electrochemical impedance spectroscopy, Electrochim. Acta 51 (2006) 1473–1479, https://doi.org/10.1016/j.electacta.2005.02.128.
- [43] M. Mouanga, P. Berçot, Comparison of corrosion behaviour of zinc in NaCl and in NaOH solutions; Part II: electrochemical analyses, Corros. Sci. 52 (2010) 3993–4000, https://doi.org/10.1016/j.corsci.2010.08.018.
- [44] J. Venezuela, M.S. Dargusch, The influence of alloying and fabrication techniques on the mechanical properties, biodegradability and biocompatibility of zinc: a comprehensive review, Acta Biomater. (2019), https://doi.org/10.1016/j.actbio. 2019.01.035
- [45] E. Mostaed, M. Sikora-Jasinska, J.W. Drelich, M. Vedani, Zinc-based alloys for degradable vascular stent applications, Acta Biomater. 71 (2018) 1–23, https://doi.org/10.1016/j.actbio.2018.03.005.
- [46] L. Liu, Y. Meng, C. Dong, Y. Yan, A.A. Volinsky, L.-N. Wang, Initial formation of corrosion products on pure zinc in simulated body fluid, J. Mater. Sci. Technol. 34 (2018) 2271–2282, https://doi.org/10.1016/j.jmst.2018.05.005.
- [47] L.-Y. Cui, Y. Hu, R.-C. Zeng, Y.-X. Yang, D.-D. Sun, S.-Q. Li, F. Zhang, E.-H. Han, New insights into the effect of Tris-HCl and Tris on corrosion of magnesium alloy in presence of bicarbonate, sulfate, hydrogen phosphate and dihydrogen phosphate ions, J. Mater. Sci. Technol. 33 (2017) 971–986, https://doi.org/10.1016/j.jmst. 2017.01.005.
- [48] A. Krezel, W. Maret, The biological inorganic chemistry of zinc ions, Arch. Biochem. Biophys. 611 (2016) 3–19, https://doi.org/10.1016/j.abb.2016.04.010.
- [49] D. Mei, S.V. Lamaka, J. Gonzalez, F. Feyerabend, R. Willumeit-Römer, M.L. Zheludkevich, The role of individual components of simulated body fluid on the corrosion behavior of commercially pure Mg, Corros. Sci. (2018), https://doi. org/10.1016/j.corsci.2018.11.011.
- [50] V. Shkirskiy, P. Keil, H. Hintze-Bruening, F. Leroux, F. Brisset, K. Ogle, P. Volovitch, The effects of L-cysteine on the inhibition and accelerated dissolution processes of zinc metal, Corros. Sci. 100 (2015) 101–112, https://doi.org/10.1016/j.corsci. 2015.07.010.
- [51] F. Peter, S. Peter, What are the essential elements needed for the determination of amino acid requirements in humans? J. Nutr. 134 (2004) 1558S, https://doi.org/ 10.1089/1096620041224003.
- [52] S.S. Ozturk, B.O. Palsson, Chemical decomposition of glutamine in cell culture media: effect of media type, pH, and serum concentration, Biotechnol. Progr. 6 (1990) 121–128. https://doi.org/10.1021/bp00002a005.
- [53] B. El Ibrahimi, A. Jmiai, L. Bazzi, S. El Issami, Amino acids and their derivatives as corrosion inhibitors for metals and alloys, Arabian J. Chem. (2017), https://doi. org/10.1016/j.arabic.2017.07.013.
- [54] K. Khan, M. Elia, Factors affecting the stability of L-glutamine in solution, Clin. Nutr. 10 (1991) 186–192, https://doi.org/10.1016/0261-5614(91)90037-D.
- [55] S. Koutsopoulos, E. Dalas, Hydroxyapatite crystallization in the presence of amino acids with uncharged polar side groups: glycine, cysteine, cystine, and glutamine, Langmuir 17 (2001) 1074–1079, https://doi.org/10.1021/la000820p.
- [56] P.H. Qin, W.C. Lu, W. Qin, W. Zhang, H. Xie, Theoretical studies on complexes of calcium ion with amino acids, Chem. Res. Chin. Univ. 30 (2014) 125–129, https:// doi.org/10.1007/s40242-014-3303-z.
- [57] M. Rashidian, A. Fattahi, Comparison of thermochemistry of aspartame (artificial sweetener) and glucose, Carbohydr. Res. 344 (2009) 127–133, https://doi.org/10. 1016/j.carres.2008.09.020.
- [58] M. Tavafoghi, M. Cerruti, The role of amino acids in hydroxyapatite mineralization, J. R. Soc. Interface 13 (2016), https://doi.org/10.1098/rsif.2016.0462.
- [59] R.Z. Legeros, C.B. Bleiwas, M. Retino, R. Rohanizadeh, J.P. Legeros, Zinc effect on the in vitro formation of calcium phosphates: relevance to clinical inhibition of calculus formation, Am. J. Dent. 12 (1999) 65–71, https://doi.org/10.1007/ s003920170032.
- [60] M. Ascencio, M. Pekguleryuz, S. Omanovic, An investigation of the corrosion mechanisms of WE43Mg alloy in a modified simulated body fluid solution: the effect of electrolyte renewal, Corros. Sci. 91 (2015) 297–310, https://doi.org/10.1016/j.corsci.2014.11.034.